Journal of Marine Science and Technology, Vol. 24, No. 6, pp. 1070-1080 (2016)
DOI: 10.6119/JMST-016-0729-1

ASSESSMENT OF LANDFORM CHANGES IN BARAMARAE TIDAL FLAT, KOREA USING COMBINED ANALYSIS OF MULTI-TEMPORAL REMOTE SENSING IMAGES AND GRAIN SIZE MEASUREMENT DATA

Yeseul Kim[1], Dong-Ho Jang[2], No-Wook Park[1], and Hee Young Yoo[3]

Key words: tidal flat, grain size, digital elevation model, remote sensing.

ABSTRACT

In this study, information on landform change in Baramarae tidal flat, Korea is analyzed using multi-temporal Landsat images and grain size measurement data. Unlike previous studies that focused on the extraction of topographic changes from intertidal digital elevation models (DEMs), information on landform change is assessed in the present study by considering both topography and surface sediment characteristics. DEMs in 2000 and 2010 were first generated using waterlines extracted from 16 Landsat images. Mean grain size distribution maps were also generated by interpolating sample data acquired in the field in 2002 and 2012. The non-spatial and spatial characteristics of the landform change in the study area were then analyzed using contingency table plots and difference maps, respectively. Overall sedimentation and coarsening of surface sediments caused by different local marine energy environments were dominant in the study area during the 10-year period. The combined analysis also revealed a close relationship between the changes in topography and grain size. Sedimentation was dominant mainly in areas with fine-grained sediments, while a coarsening trend in the sediments increased with elevation. Moreover, it was possible to locate specific areas in which erosion and a fining trend of surface sediments were observed, which differed from the overall trend of change in the study area. These case study results indicate that the combined analysis of both topography and surface sediment characteristics is very useful in the exploration and monitoring of landform changes in tidal flats.

Paper submitted 02/25/16; revised 03/25/16; accepted 07/29/16. Author for correspondence: No-Wook Park (e-mail: nwpark@inha.ac.kr).
[1] Department of Geoinformatic Engineering, Inha University, Incheon, Korea.
[2] Department of Geography, Kongju National University, Gongju, Korea.
[3] Geoinformatic Engineering Research Institute, Inha University, Incheon, Korea.

I. INTRODUCTION

Tidal flats, such as those developed along the west coast of the Korean Peninsula, are invaluable transition and productive zones that have undergone continuous environmental changes (Ryu et al., 2002; Park et al., 2009; Xu et al., 2013). Changes of topography and sediment characteristics in tidal flats are due mainly to changes in tidal currents and wave patterns by sediment budget processes, marine energy processes, and coastal construction activities (Ryu et al., 2008; Park et al., 2009). These landform changes may be accelerated in the long term by sea level rise through climate change. The ecosystem and human activity in tidal flats are greatly affected by environmental changes. Thus, periodic monitoring of the landform environments in tidal flats is of great importance for the systematic management of coastal zones.

Because accessibility to tidal flats is limited, due mainly to the short exposure time between tides and issues related to operating in mud, it is very difficult to obtain a sufficient number of periodic observational datasets for environmental change monitoring through field surveys only. Such limited observations are insufficient to analyze the characteristics and patterns of overall changes in tidal flats. To overcome these limitations, remote sensing data, which can provide both periodic and regional information, can be a useful source for thematic mapping in tidal flats. Various studies have been conducted that are based on the analysis of remote sensing data for monitoring landform changes (Ryu et al., 2008; Heygster et al., 2010; Xu et al., 2013), determining surface sediment characteristics (Van der Wal and Herman, 2007; Park et al., 2009; Choi et al., 2010), and conducting ecological research (Van der Wal et al., 2008; Choi et al., 2011).

Among the aforementioned application fields of remote sensing in tidal flats, the present study focuses mainly on the extraction of quantitative information on landform changes in tidal flats. Comparison of digital elevation models (DEMs) generated at different times is a simple yet efficient method for

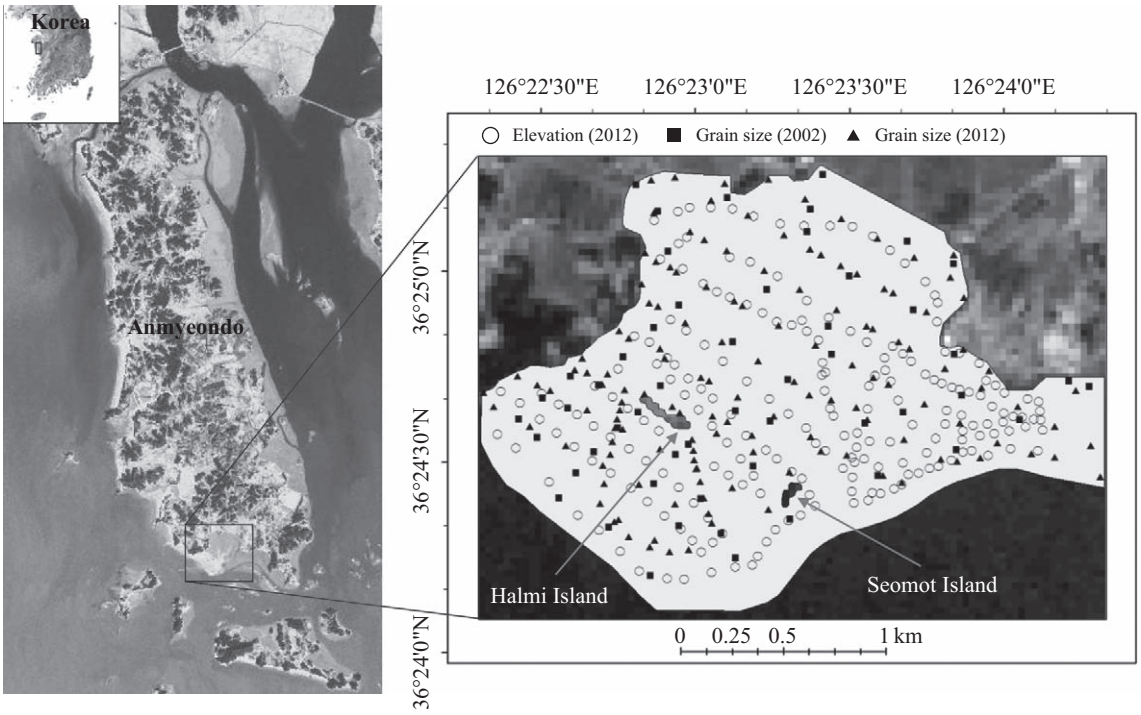

Fig. 1. Location map of the study area and ground survey sample points.

extracting information on erosion and sedimentation in tidal flats. The intertidal DEMs have been generated using various image data sources and methods, such as synthetic aperture radar (SAR) interferometry (Wimmer et al., 2000; Park et al., 2012), LIDAR (Stockdon et al., 2002; Deronde et al., 2006; Noernberg et al., 2010), and a waterline method (Mason et al., 1995, 1998; Ryu et al., 2002; Lee and Kim, 2004; Heygster et al., 2010; Kim et al., 2013a; Xu et al., 2013). The waterline method is a widely applied technique, in which the waterline is the boundary between a water body and exposed tidal flats, and represents an equal tidal height or elevation line at the time of image acquisition (Mason et al., 1995). Thus, topographic information on tidal flats can be generated by stacking many waterlines extracted under various tidal conditions. By comparing such DEMs generated at different times, information on landform change such as erosion and sedimentation can be easily obtained.

Previous studies have focused mainly on the generation and comparison of DEMs for landform monitoring in tidal flats. If quantitative analysis on the characteristics of surface sediments such as grain size is accompanied by information on topographic change, a much richer interpretation of landform change is possible. To our knowledge, very few studies have combined the analysis of changes in the topography with grain size of the surface sediments (Kim et al., 2013b). Although Kim et al. (2013b) attempted this combined analysis, only a simple qualitative comparison of the DEMs and grain size distributions was undertaken.

The main objective of the present study is such a quantitative combined analysis, in which the assessment of landform change in the tidal flats is performed using multi-temporal remote sensing images and grain size measurement data. First, the DEMs in tidal flats are generated using waterlines extracted from multi-temporal remote sensing images. Topographic change information such as sedimentation or erosion is extracted by comparing the DEMs generated at different times. To relate the changes in topography to changes in the characteristics of the surface sediments, grain size distributions are also generated from field sampling and laboratory measurement. By combining the information on topographic and grain size changes, landform change can be interpreted both quantitatively and qualitatively. A case study of Baramarae tidal flat in Korea was conducted to examine the applicability and potential of the combined analysis using both DEMs from time-series Landsat images and grain size data from field surveys.

II. MATERIALS AND METHODS

1. Materials

1) Study Area

The case study area is Baramarae tidal flat in the southern part of Anmyeondo, Korea, which is located on the west coast of the Korean Peninsula, as shown in Fig. 1. The coastal geomorphology near the study area corresponds to a typical rias coast. Tidal flats and beaches are widely developed in the study area due to the indented coastline. The occurrence of two sea stacks including Halmi and Seomot Islands, a wave-cut platform, and sand dunes at the indentation in the coast have impeded ocean waves resulting in the development of large tidal flats. Ocean waves and tidal currents have also contributed to

Table 1. List of Landsat data used for the generation of DEMs.

No	Satellite Sensor	Acquisition date (mm/dd/yyyy)	Tidal level (cm)	Height (cm)	Tide condition	Remark
1	Landsat-5 TM	03/20/2000	-45	-397.43	Flow	DEM 2000
2	Landsat-5 TM	08/11/2000	295	-34.94	Flow	
3	Landsat-5 TM	03/23/2001	56	-264.30	Flow	
4	Landsat-5 TM	04/24/2001	-10	-378.32	Flow	
5	Landsat-5 TM	09/15/2001	248	-58.80	Flow	
6	Landsat-7 ETM+	01/29/2002	-75	-418.77	Flow	
7	Landsat-7 ETM+	06/06/2002	424	54.59	Flow	
8	Landsat-5 TM	06/14/2002	187	-223.23	Ebb	
9	Landsat-7 ETM+	04/06/2003	154	-255.81	Ebb	
10	Landsat-7 ETM+	04/22/2009	266	-41.68	Flow	DEM 2010
11	Landsat-5 TM	06/01/2009	510	116.33	Ebb	
12	Landsat-7 ETM+	06/25/2009	116	-294.45	Ebb	
13	Landsat-7 ETM+	01/03/2010	-55	-449.45	Ebb	
14	Landsat-7 ETM+	04/28/2011	379	39.39	Flow	
15	Landsat-7 ETM+	09/03/2011	203	-220.63	Ebb	
16	Landsat-7 ETM+	06/17/2012	221	-98.83	Flow	

the development of these tidal flats (Park et al., 2009; Park and Jang, 2014). The ocean waves generated by the monsoon affected the development of the beach and tidal flats with a high sand and gravel content near Halmi Island and in the western part of the study area. The sources of the sediments in these areas are periglacial sediments from nearby mountains and marine deposits. Deposits in the inner bay originated from terrigenous weathered materials from nearby mountains. Moreover, very fine-grained materials were deposited on these terrigenous weathered materials overlying the bedrock near the coastline. After the bedrock surface was weathered, sediments in the tidal flats were gradually deposited by the effects of tidal currents (Kim and Jang, 2011). In relation to the sedimentation and erosion processes in the study area, Kim and Jang (2011) reported that sedimentation is relatively dominant in fall, whereas erosion is dominant in spring.

The tides in the study area are semi-diurnal with a mean tidal range of about 4.6 m. The mean tidal current velocities near the study area are about 0.8 m/s and 0.9 m/s during flood and ebb tides, respectively (Park and Jang, 2014). The flood current flows between Halmi and Seomot Islands 2 hours after low tide in a north-south direction. The ebb current flows out between Halmi and Seomot Islands from the indentation, and partly in a southeast direction to the east of Seomot Island (Khodadad and Jang, 2014).

2) Datasets

A total of 16 cloud-free satellite images of the study area, including 7 Landsat-5 Thematic Mapper (TM) images and 9 Landsat-7 Enhanced Thematic Mapper Plus (ETM+) images, acquired under various tidal conditions were collected in order to generate the DEMs (Table 1). Data gaps occur in Landsat-7 ETM+ images acquired after May 31, 2003, due to a scan line corrector (SLC) failure. However, because the study area is located in the center of the full scene, it is not affected by the data gaps in SLC-off data (Markham et al., 2004). The nine images acquired from March 2000 to April 2003 were used to extract waterlines for the construction of the DEM circa 2000, hereafter referred to as DEM 2000. DEM 2010 was constructed using waterlines extracted from seven images acquired from April 2009 to June 2012. All images were geometrically rectified using a digital topographic map and pre-rectified images.

Ground-based elevation data collected in February 2012 (Fig. 1) were used for assessment of the accuracy of DEM 2010. A NetWork RTK X90 GPS with ±10 mm horizontal and ±20 mm vertical accuracy was used for elevation measurement. To calibrate the different local coordinate systems, site calibration was implemented using a local coordinate system based on a bench-mark located at Gonam Elementary School. Several measurement points were excluded that are located not only near the boundaries between land and tidal flats, but also at sand dune areas near Halmi Island that are always exposed regardless of tidal conditions. Ultimately, 207 points were used for the assessment of elevation accuracy.

Other data used in this study include surface sediment samples obtained for mapping grain size change in the surface sediments, including 53 and 140 samples collected in February 2002 and 2012, respectively. After removal of organic materials and carbonates, the Mastersizer 2000 particle-sizing instrument was used to determine the mean grain size of each sample.

2. Methods

1) DEM Generation

The DEMs in this study were generated using the waterline extraction method widely used for generating DEMs of tidal

flats. Generally, infrared bands, which show very low reflectance values in a water body, can be used effectively for extracting waterlines. However, the typical reflectance pattern in infrared bands may vary according to tidal conditions. During an ebb tide, the shortwave infrared (SWIR) band is significantly more affected by surface remnant water on exposed tidal flats than the near infrared (NIR) band (Ryu et al., 2002). Therefore, different combinations of NIR and SWIR bands were applied to extract waterlines during flood and ebb tides. NIR and SWIR bands were both used for images acquired during flood tides, whereas only the NIR band was used for images acquired during ebb tides. Although the thermal infrared band is also reported to be effective for waterline extraction (Ryu et al., 2002), it was not considered because of its poor spatial resolution of 60 m and 120 m for Landsat TM and Landsat ETM+, respectively. On the basis of the characteristics of the different band combinations, a density slicing method was first applied as a preliminary step and the waterlines were subsequently extracted in a vector format by manual on-screen digitizing based on visual inspection.

Once the waterlines were extracted, a height value was assigned to each waterline. The height value for each waterline was computed using three data sources: (1) tide height at the time of image acquisition at the Boryeong tidal station which is the tide gauge station in the closest proximity to the study area; (2) the correction constants for Sodo in tide tables; and (3) the mean sea level difference between the study area and the Incheon standard port. After the height value based on these three sources was assigned to each waterline, DEM 2000 and DEM 2010 were finally generated in a raster format by applying the Topo to Raster tool in ArcGIS 10.3 software.

A lack of ground-based elevation measurements in 2000 prevented quantitative validation of DEM 2000. However, because the same sensor data and procedure for generating DEM 2010 was applied to DEM 2000, we have assumed that the overall characteristics of errors in DEM 2010 were the same as those in DEM 2000. Under this assumption, the error calibration procedure based on the validation result of DEM 2010 was then applied. Because ground-based elevation data are available only for DEM 2010, the relationship between the true elevation and DEM 2010 at field survey locations was first modeled to calibrate both primitive DEMs. If a linear relationship was observed, simple linear regression was applied to derive the quantitative relationship between the true elevation and DEMs generated from the waterline method. If a strong non-linear relationship was found between the true elevation and the DEM, non-linear regression models that fit well to the non-linear relationship could be applied to derive the quantitative relationship. This modeling result was then applied to calibrate both of the primitive DEMs. The main focus of this study is to assess the relative trend in landform changes during a 10-year period by comparing the two DEMs. Therefore, this calibration approach was adopted considering the data availability, although non-negligible errors were still included in both DEMs.

After applying the calibration approach, the elevation change information was obtained by subtracting the calibrated DEM 2000 from the calibrated DEM 2010.

2) Grain Size Mapping

To generate the spatial distribution of mean grain size across the study area, ordinary kriging, which can account for spatial autocorrelation and directional variability in spatial interpolation (Goovaerts, 1997; Deutsch and Journel, 1998), was applied to the interpolation of the sample data.

Suppose that $\{z(\mathbf{u}_\alpha), \alpha = 1, \ldots, n\}$ is the set of grain size measured at n sampling locations $\mathbf{u}_\alpha$. In geostatistics, spatial autocorrelation is quantified by variogram denoted by $\gamma(\mathbf{h})$, such that:

$$\gamma(\mathbf{h}) = \frac{1}{2N(\mathbf{h})} \sum_{\alpha=1}^{N(\mathbf{h})} [z(\mathbf{u}_\alpha) - z(\mathbf{u}_\alpha + \mathbf{h})]^2 \tag{1}$$

where $N(\mathbf{h})$ is the number of pairs of sample data locations separated by the lag distance vector $\mathbf{h}$. Because the variogram is a function of both distance and direction, it can account for anisotropic spatial autocorrelation structures (Deutsch and Journel, 1998).

Ordinary kriging predicts grain size values at unsampled locations ($\mathbf{u}$) as a linear combination of neighboring sample data:

$$z^*(\mathbf{h}) = \sum_{\alpha=1}^{n(\mathbf{u})} \lambda_\alpha(\mathbf{u}) z(\mathbf{u}_\alpha) \text{ with } \sum_{\alpha=1}^{n(\mathbf{u})} \lambda_\alpha(\mathbf{u}) = 1 \tag{2}$$

where $\lambda_\alpha(\mathbf{u})$ is an ordinary kriging weight assigned to the neighboring sample data and $n(\mathbf{u})$ is the number of sampled data within the predefined search window.

The ordinary kriging weight is determined by solving the following ordinary kriging system (Goovaerts, 1997):

$$\begin{aligned} &\sum_{\beta=1}^{n(\mathbf{u})} \lambda_\beta(\mathbf{u}) \gamma(\mathbf{u}_\alpha - \mathbf{u}_\beta) - \mu(\mathbf{u}) = \gamma(\mathbf{u}_\alpha - \mathbf{u}) \quad \alpha = 1, \ldots, n \\ &\sum_{\beta=1}^{n(\mathbf{u})} \lambda_\beta(\mathbf{u}) = 1 \end{aligned} \tag{3}$$

where $\mu(\mathbf{u})$ is the Lagrangian parameter to ensure the constraint on the unity sum of the weights, and $\gamma(\mathbf{u}_\alpha - \mathbf{u}_\beta)$ and $\gamma(\mathbf{u}_\alpha - \mathbf{u})$ are variogram values between two sample locations and between sample and estimation locations, respectively.

For grain size mapping, it is assumed that the distributions of the mean grain sizes in 2002 and 2012 represent the characteristics of surface sediments in 2000 and 2010, respectively. By computing the difference in grain sizes between 2002 and 2012, the changes in grain sizes during the elapsed time period (i.e., 10 years) were calculated.

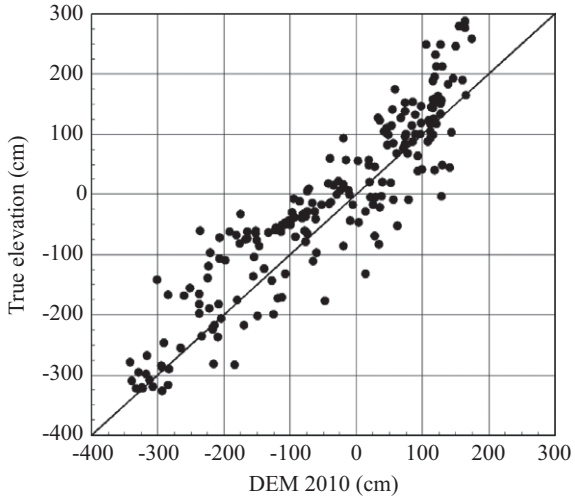

Fig. 2. Scatterplot of true elevations against elevations from DEM 2010.

III. RESULTS

1. DEM Generation

After extracting the waterlines from the multi-temporal Landsat images, primitive DEMs in a raster format were generated, nominally for 2000 and 2010. A comparison of the elevations from DEM 2010 with true elevations was made for accuracy assessment. The mean error (ME) and mean absolute error (MAE) were computed to measure the degree of bias and the magnitude of errors, respectively. The ME and MAE values were -25.17 cm and 49.93 cm, respectively. The negative ME value indicates that overall, DEM 2010 tended to unde restimate the true elevation.

As shown in Fig. 2, a strong non-linear relationship was not observed in the scatterplot, even though high elevation values were not reproduced in DEM 2010. The linear correlation coefficient value is 0.92, which indicates a strong linear relationship between the true elevations and DEM 2010. To examine the assumption of this linear relationship, an additional test was conducted to compare the overall fit of the linear regression with that of a non-linear model. A generalized additive model (Hastie and Tibshirani, 1990) was chosen as the non-linear statistical model because of the weak non-linear relationship. To avoid overfitting, other complex non-linear models, such as support vector regression and neural networks, were not considered in this study. The predictive performance was measured using the deviance accounted for by the model (D^2) which was computed by (null deviance - residual deviance)/null deviance, and is equivalent to R^2 in linear models. The D^2 value for the generalized additive model was 0.86, which is very similar to the R^2 value of 0.85 for linear regression. On the basis of this test result, the simple linear regression was ultimately selected to calibrate the primitive DEMs due to its simplicity and efficiency.

The linear relationship between the true elevation and DEM 2010 was modeled as true elevation = 0.923 × DEM 2010 + 24.56. By applying this linear regression model to both of the primitive DEMs, the two calibrated DEMs were finally obtained (Fig. 3). As shown in Fig. 3(a), the elevation of most areas in 2000 ranged between 0 cm and 200 cm. Areas with elevation greater than 200 cm were located in an embayment inside Halmi Island, and in sand bars and sand spits developed along its periphery. Moreover, the overall elevation in the seaward areas was below mean sea level, and the elevation and slope decreased along the southwestern seaward areas. In DEM 2010 (Fig. 3(b)), high-elevation areas greater than 200 cm had been enlarged along the embayment, sand bar, and sand spit. An increase in elevation was also found near the sand spit in northeastern Seomot Island, whereas the elevation along the seaward areas and tidal waterway decreased slightly.

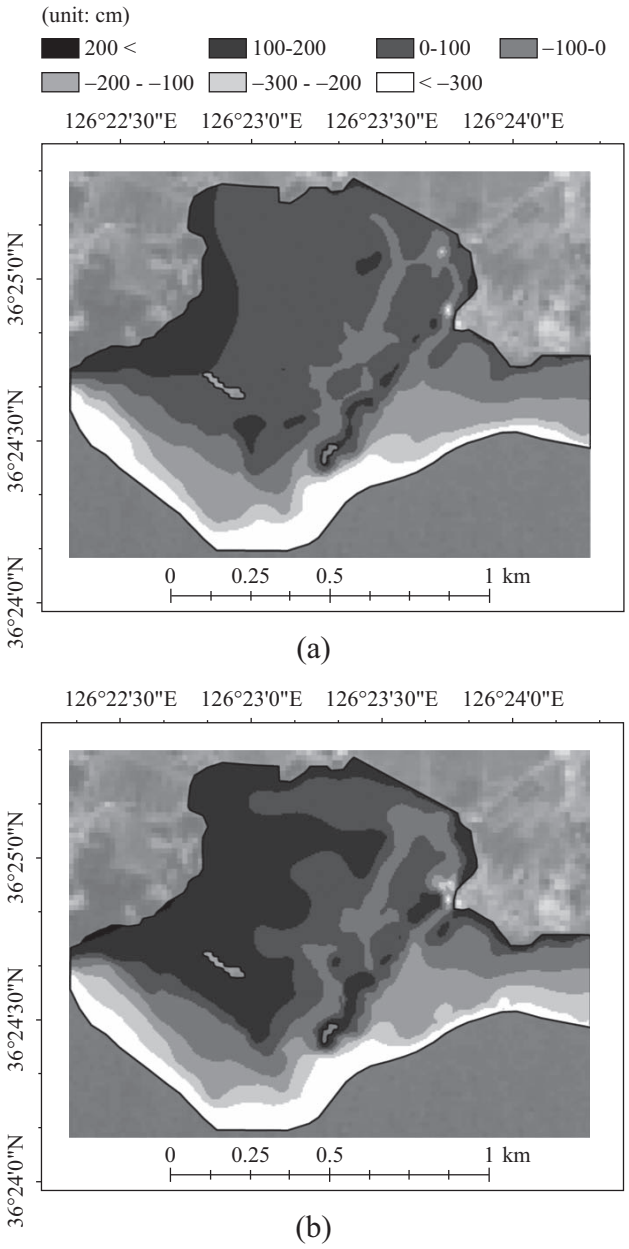

Fig. 3. Calibrated DEMs in (a) 2000 and (b) 2010.

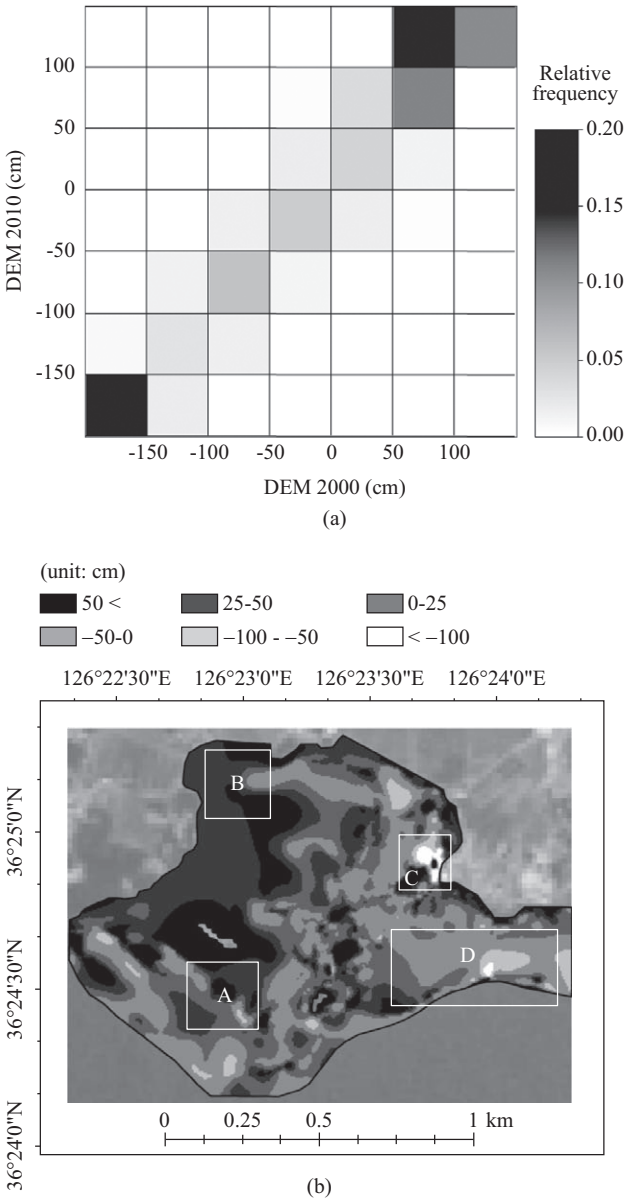

Fig. 4. (a) Contingency table plot of elevations between DEM 2000 and DEM 2010; (b) elevation change map between 2000 and 2010.

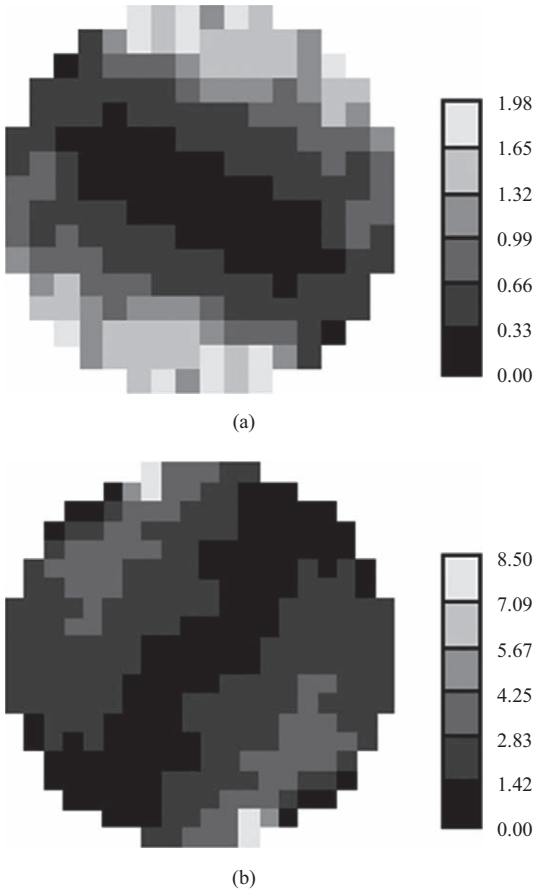

Fig. 5. Variogram maps of grain sizes of samples in (a) 2002 and (b) 2012.

To explore the topographic changes between 2000 and 2010, a contingency table plot was generated to display the frequencies of the cross-classified data elements (Agresti, 2012). Fig. 4(a) shows that the area in which the elevation ranged between 50 cm and 100 cm in DEM 2000 changed to elevations greater than 100 cm in DEM 2010. This result shows that sedimentation was dominant in this elevation interval during the 10-year study period.

The spatial distribution of elevation changes between 2000 and 2010 was generated by subtracting DEM 2000 from DEM 2010. In Fig. 4(b), locally different patterns in sedimentation and erosion are apparent. Sedimentation was dominant near Halmi Island (Area A), with a high sand and gravel content, and in the northwest embayment (Area B). Strong sedimentation, greater than 50 cm in terms of the elevation change, was observed near the sand spit in northern Seomot Island and at the southern part of the beach (Area A). This deposition was caused by the accumulation of eroded sediments from the seaward area and tidal waterway. In particular, the growth in the tidal sand bar by the northwestern monsoon also contributed to deposition in the southern part of the beach. Meanwhile, erosion was dominant along the tidal waterway (Area C) and in the eastern seaward areas (Area D). The dominant erosional trend in these areas occurred because the stronger velocity of the tidal current hindered the accumulation of sediments along the tidal waterway. In addition, the embankment in the inner bay hindered the movement and supply of sediments. In particular, the increase in velocity of the tidal current resulted in accelerated erosion in Area D. The increase in velocity along the tidal waterway also contributed to the predominance of erosion near the tidal creek and tidal depression in Area C.

2. Grain Size Mapping

All geostatistical analyses were implemented using the geostatistical analyst in ArcGIS and Fortran programming. To explore the directional variability of the grain size distributions, variogram maps (Goovaerts, 1997) were first computed. As indicated by the variogram maps shown in Fig. 5, the grain

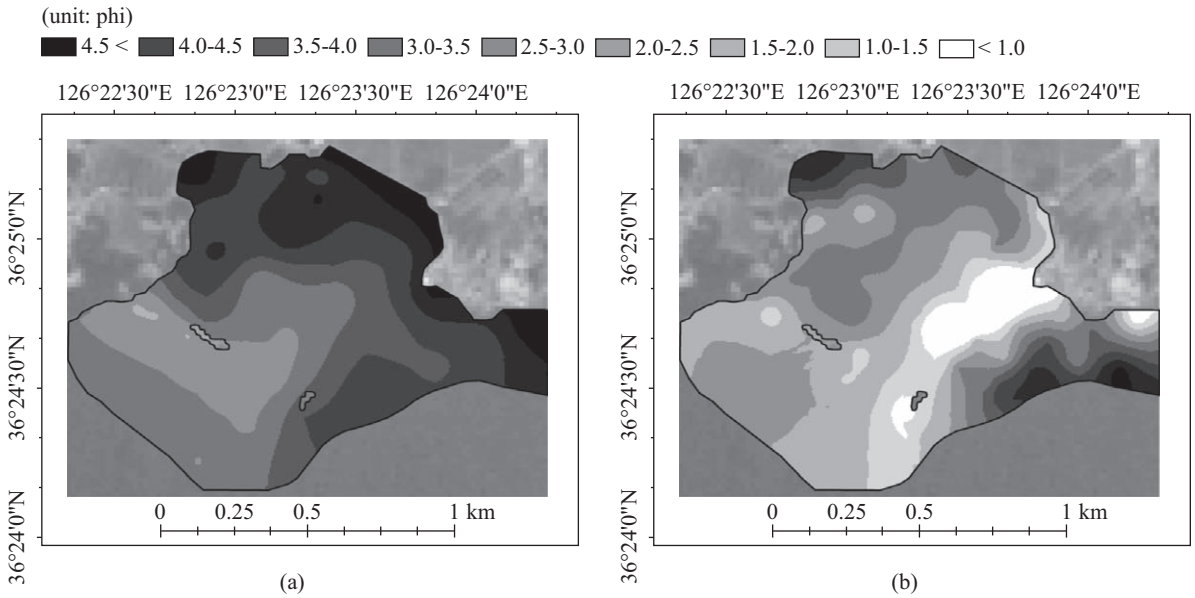

Fig. 6. Spatial distribution of grain sizes in (a) 2002 and (b) 2012.

size datasets in both 2002 and 2012 showed different anisotropy patterns. That in 2002 showed a strong anisotropy in the NW-SE direction, whereas that in 2012 showed anisotropy along the NE-SW direction. The different anisotropic patterns between 2002 and 2012 imply that the direction-dependent variability in grain size changed significantly during the 10-year period. The direction of the anisotropy in 2002 corresponds to that of tidal currents. A field survey revealed a NW-SE direction in the ripple marks in the study area during flood and ebb currents, implying that the sorting of sediments was also affected by the direction of tidal currents. As a result, the anisotropic pattern was observed along the same direction in 2002. The different anisotropy direction in 2012 is attributed to the change in flow direction of the tidal currents. Sand bars newly developed in the southeastern area blocked the flood current in the NW-SE direction and caused the current to flow westward. After joining in the open sea, the tidal currents flowed in the NE-SW direction along the tidal waterway between Halmi and Seomot Islands. As a result, the sorting of sediments also showed a NE-SW anisotropic pattern similar to the direction of the tidal currents.

After variogram modeling with the anisotropy model, ordinary kriging was applied to generate the grain size distribution maps for 2002 and 2012. Leave-one-out cross validation was implemented to quantify the prediction performance of ordinary kriging. The MAE values for 2002 and 2012 were 0.35 and 0.75, respectively.

The grain size distributions in 2002 and 2012 are presented in Figs. 6(a) and (b), respectively. As expected from the variogram analysis, continuity along the main directions of anisotropy was observed in the ordinary kriging results. In 2002, fine-grained sediments were distributed mainly near the embayment area, whereas coarse-grained sediments were dominant along the NW-SE direction in the seaward areas. In particular, the beach areas near Halmi Island, in addition to some sand bars and sand spits, are clearly represented in the results. Most sediments in 2012 were coarser than those in 2002, and a distinct coarsening trend was found along the tidal waterway. In contrast, the grain sizes in the eastern seaward areas were finer than those in 2002. A decrease in the velocity of ocean waves could have caused the fine-grained surface sediments from Cheonsu Bay to be transported east of the study area.

The changes in grain size between 2002 and 2012 were further explored by generating the contingency table plot shown in Fig. 7(a). As expected, a coarsening trend is clearly shown in the plot. A decrease in the mean grain size in phi units (φ) was dominant in the fine-grained sediments from 2002. The most significant decrease of the mean grain size in phi units was observed in the grain size interval between 2.0 and 3.0 φ in 2002.

By subtracting the grain size values obtained in 2002 from those obtained in 2012, the spatial distribution of grain size change between 2002 and 2012 was generated, as shown in Fig. 7(b). As revealed in Fig. 7(a), the overall grain size in the study area decreased in phi units, which shows that most of the sediments became coarser during the 10-year period. This trend was particularly dominant near the tidal waterway (Area C). Sediments in this area showed the characteristics of granules created by strong erosion by tidal currents. The front and back areas around Halmi Island (Area A) also showed a coarsening trend. Because the southwest areas are connected to the open sea, erosion in the high-energy environment was dominant. The coarse-grained sediments that were transported from the tidal waterway during the ebb current contributed to the coarsening trend in these areas. Due to the increase in tidal energy caused by sea level rise, coarse-grained sediments could have been transported into the northwest region of the embayment.

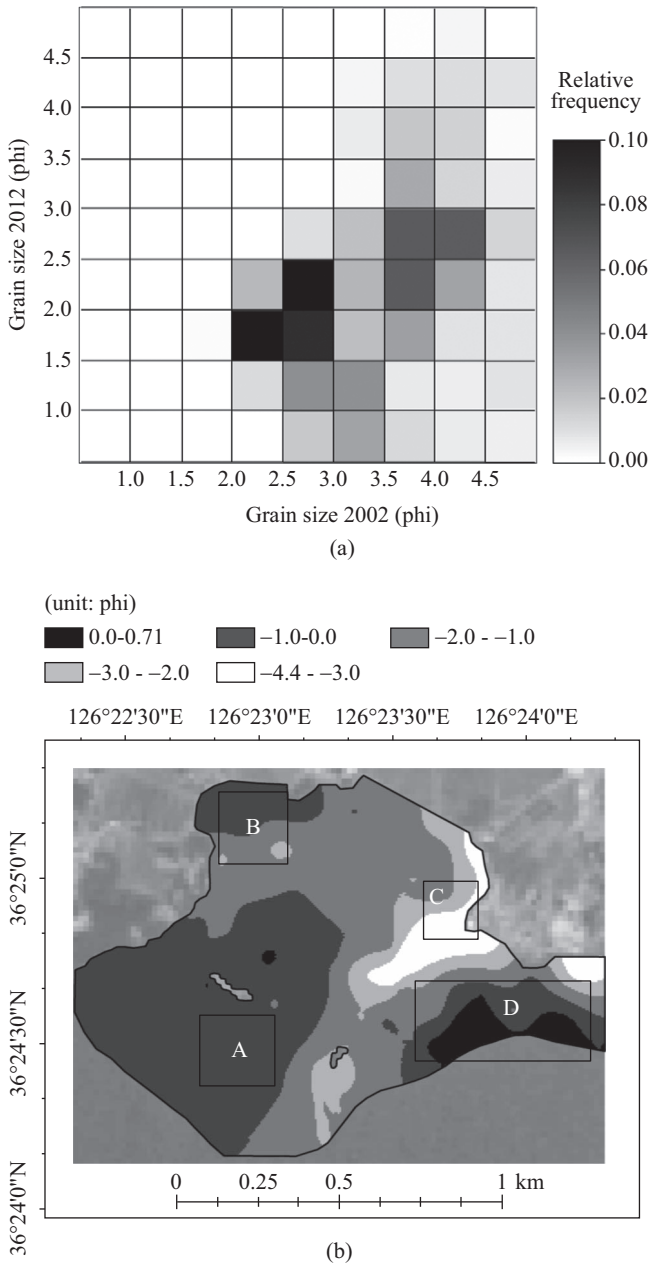

Fig. 7. (a) Contingency table plot of grain sizes between 2002 and 2012; (b) grain size change map between 2002 and 2012.

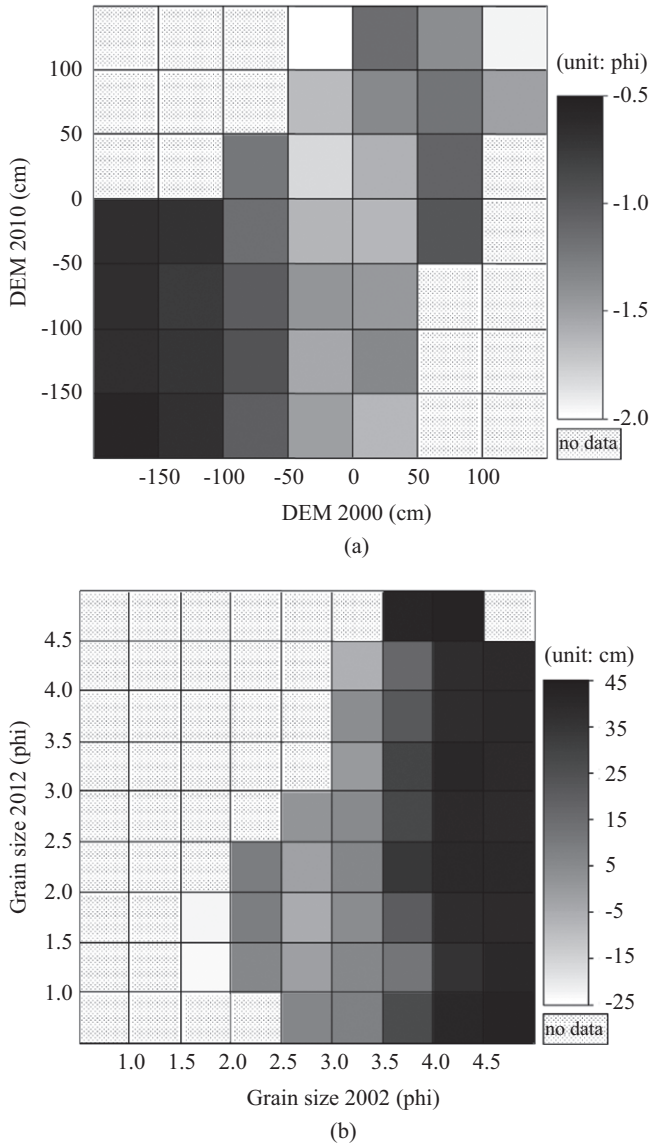

Fig. 8. Contingency table plots of (a) grain size changes between elevation values in DEM 2000 and DEM 2010; (b) elevation changes between grain size values in 2002 and 2012.

As a result, a coarsening trend was developed in Area B. In contrast, the fining trend observed in Area D can be explained by the low-energy environment. Although Area D is connected to the open sea, other tidal flats located in the front part of Area D blocked the ocean waves, thus allowing the deposition of fine-grained surface sediments from Cheonsu Bay.

3. Combined Analysis of Topographic and Grain Size Change

Thus far, separate interpretations have been given for the changes in topography and grain size. In this subsection, combined interpretations of both variables were performed by constructing different contingency table plots. Unlike the contingency table plots shown in Figs. 4(a) and 7(a), which represent relative frequencies, the contingency table in Fig. 8(a) shows the average grain size change values between DEM 2000 and DEM 2010. In addition, the average topographic change values between grain size classes in 2002 and 2012 are displayed in the contingency table in Fig. 8(b).

In Fig. 8(a), a weak coarsening trend is shown in low-elevation areas below mean sea level. As the elevation increased, the average grain size decreased in phi units, that is, the coarsening trend became stronger. In the embayment with high elevation, coarse-grained sediments that were continuously transported into this area from the open sea contributed to this coarsening

trend. Moreover, the trends in sedimentation and erosion were mixed in the seaward area with low elevation, due to an increase in ocean wave energy and tidal currents.

The results in Fig. 8(b) indicate that increases in elevation changes are exhibited by most areas of fine-grained sediments in 2002. The elevation in tidal flat areas with fine-grained sediments increased through the continuous supply of sediments from the open sea. Moreover, areas with significant erosion contained coarse-grained sediments with a mean grain size below 2.0 φ.

Despite the potential of the combined analysis, the non-spatial nature of the analysis based on contingency table plots is limited in determining the spatial characteristics of landform changes. To account for the spatial nature of landform changes, further interpretations were made by simultaneously considering the changes shown in Figs. 4(b) and 7(b). Coarse-grained sediments that were transported from the open sea were deposited in Areas A and B. Thus, the elevation increased in these areas during the 10-year period. In Areas C and D, the increase in energy of the ocean waves and the tidal currents resulted in a decrease in elevation through erosion. However, these areas showed different characteristics in terms of grain size change. The sediments in Area C became significantly coarser due to the strong erosion, whereas a fining trend was detected in Area D, although erosion was dominant there. This difference is attributed mainly to the particular location of Area D relative to the open sea, which is different from the general landform environment of tidal flats. Other tidal flats located in the seaward part of Area D also provided sources for the fining trend. Area D exhibits landform change patterns that differ significantly from those in other areas. Recently, Khodadad and Jang (2014) reported that erosion is accelerated in this area due to the effects of artificial mooring facilities and their effects locally on tidal energy. Therefore, it is considered necessary to monitor the change patterns in Area D.

On the basis of the results of the combined analysis, it is confirmed that the elevation changes are closely related to grain size change in the study area, which could not be proved from separate analyses of the changes in topography and grain size.

IV. DISCUSSION

Regarding the generation of DEM, it is assumed that the topographic change during the period of data acquisition was negligible, as is assumed in the waterline method (Ryu et al., 2008). As discussed by Ryu et al. (2008), however, the coastal dynamics of annual and seasonal changes may not be negligible. In the present study, spring images acquired from March through June, including six of the nine images in DEM 2000 and five of the seven images in DEM 2010, were collected mainly to reduce the seasonal change effect. However, some summer and winter images were still included to extract additional waterlines. Despite this weakness, the above mentioned assumption was adopted because the assessment of overall patterns of landform changes during the 10-year period is the main objective of this study.

Relatively large error statistics of DEM were caused by a lack of sufficient waterlines representing the topographic variations in the study area due to weather conditions in addition to the temporal resolution of Landsat data, which is a common limitation of the waterline method. It may be argued that the errors of DEM 2010 are not negligible for interpretations. However, compared with the validation result of Ryu et al. (2008), in which ground leveling data along only two profiles were used, the present study used a substantially greater number of validation points (i.e., 207) scattered in the study area. As discussed by Kim et al. (2013a), the locally varying degree of relief in the study area and the spatial resolution of Landsat images (i.e., 30 m) may have caused relatively large errors in the accuracy assessment results with many validation points. When considering the range value of about 615 cm in true elevation, however, these error statistics were considered to be acceptable for the assessment of the relative trend of elevation changes during the 10-year period.

The landform changes in the study area were caused mainly by marine energy processes. However, the effect of climate change may act as an additional driving force of environmental changes in the study area. In particular, sea level rise can be a source of potential shoreline retreat and coastal inundation. Because tidal flats are widely used for economic activity and recreation, such changes will result in a socio-economic impact or even a loss of tidal flats. To mitigate this potential problem in the long term, remote sensing could be very valuable for consistent monitoring and management. However, despite the great potential of remote sensing, it should be noted that the thematic information extracted from remote sensing data is not error-free. In change detection or monitoring, errors inherent to thematic information strongly affect the analysis results, leading to error propagation problems. Thus, to extract reliable thematic information from remote sensing, the use of observations based on remote sensing data should be accompanied by the development of advanced data processing techniques in addition to proper accuracy assessment and validation based on field survey.

Because of the lack of the validation data for DEM 2000 in this study, a simple calibration approach based on the quantitative relationship in 2010 was applied to both primitive DEMs. The main limitation of this approach is that the spatial nature of ground truth data is ignored for the correction of errors in DEM. If ground truth data are available for the two DEM generation intervals, their integration with the primitive DEMs can be accomplished by multivariate kriging to produce more reliable elevation information. This data integration approach can also be extended to grain size mapping. If only field survey data are used for grain size mapping, the local detailed patterns cannot be captured in the interpolation result. As shown by Park et al. (2009), multivariate kriging can be applied to incorporate high resolution remote sensing data into grain size mapping. The detailed and reliable mapping of grain size patterns can improve interpretations of grain size change; thus, detailed relationships of the changes in topography and grain size can be

determined.

In relation to error propagation problems, a probabilistic approach that can account for the uncertainty attached to thematic mapping should also be considered. If both ground survey data and remote sensing images are available, geostatistical simulation can be effectively applied to generate alternative realizations, and thus spatial uncertainty can be quantified for decision-making. This approach has great potential in many thematic mapping tasks such as coastal inundation vulnerability mapping (Kim et al., 2013a; Leon et al., 2014).

V. CONCLUSIONS

This study has demonstrated the potential of the combined use of remote sensing images and field survey data for quantitative assessment of landform changes in tidal flats. Most previous studies that detected topographic changes from remote sensing images were based solely on the comparison of DEMs. In the present study, however, two different but linked characteristics, i.e., sedimentation and erosion, were extracted from topography and surface sediment data and then combined.

The results of the case study illustrate the possibility of linking sedimentation or erosion patterns extracted from the comparison of DEMs with grain size change occurring over a prolonged period, such as the 10 years here. Although locally different trends in landform changes were observed in the study area, non-spatial statistical information as well as information relating to the spatial characteristics of overall change, could be extracted from the contingency table plots and the comparison of change maps, respectively. Dominant sedimentation in most of the areas of fine-grained sediments, the majority of which became coarser. Moreover, it was possible to find areas in which quite different landform changes (i.e., erosion and a fining trend) were accelerated by changes in energy environments caused by the construction of artificial facilities.

In general, research on climate change impact and vulnerability requires numerous time-series datasets to enable the analysis of change. Periodic field surveys have been conducted to acquire elevation and grain size data since 2012, and high-resolution remote sensing images in the study area have been also collected during the same period. Thus, the potential of the aforementioned advanced data processing techniques for the monitoring of tidal flats will be evaluated in future work.

ACKNOWLEDGMENTS

This work was supported by Basic Science Research Program through the National Research Foundation of Korea (NRF) funded by the Ministry of Science, ICT & Future Planning (NRF-2015R1A1A1A05000966).

REFERENCES

Agresti, A. (2012). Categorical Data Analysis. Wiley, New Jersey.

Choi, J.-K., H.-J. Oh, B.-J. Koo, S. Lee and J.-H. Ryu (2011). Macrobenthos habit mapping in a tidal flat using remotely sensed data and a GIS-based probabilistic model. Marine Pollution Bulletin 62(3), 564-572.

Choi, J.-K., J.-H. Ryu, Y.-K. Lee, H.-R. Yoo, H.-J. Woo and C.-H. Kim (2010). Quantitative estimation of intertidal sediment characteristics using remote sensing and GIS. Estuarine. Coastal and Shelf Science 88(1), 125-134.

Deronde, B., R. Houthuys, W. Debruyn, D. Fransaer, V. V. Lancker and J. P. Henriet (2006). Use of airborne hyperspectral data and laser scan data to study beach morphodynamics along the Belgian Coast. Journal of Coastal Research 22(5), 1108-1117.

Deutsch, C. V. and A. G. Journel (1998). GSLIB: Geostatistical Software Library and User's Guide. Oxford University Press, New York.

Goovaerts, P. (1997). Geostatistics for Natural Resources Evaluation. Oxford University Press, New York.

Hastie, T. J. and R. J. Tibshirani (1990). Generalized Additive Models. Chapman and Hall, London.

Heygster, G., J. Dannenberg and J. Notholt (2010). Topographic mapping of the German tidal flats analyzing SAR images with the waterline method. IEEE Transactions on Geoscience and Remote Sensing 48(3), 1019-1030.

Khodadad, S. and D.-H. Jang (2014). Analysis of landform changes and sedimentary environment characteristics during winter season around the Baramarae beach, Anmyeondo in Korea's west coast. Journal of the Korean Geomorphological Association 21(1), 95-109. (in Korean, with English Abstract)

Kim, J.-S. and D.-H. Jang (2011). Time-series analysis of Baramarae beach in Anmyeondo using aerial photographs and field measurement data. Journal of the Korean Geomorphological Association 18(2), 39-51. (in Korean, with English Abstract)

Kim, Y., N.-W. Park, D.-H. Jang and H. Y. Yoo (2013a). Error analysis of waterline-based DEM in tidal flats and probabilistic flood vulnerability assessment using geostatistical simulation. Journal of the Korean Geomorphological Association 20(4), 85-99. (in Korean, with English Abstract)

Kim, Y., H. Y. Yoo, N.-W. Park and D.-H. Jang (2013b). Detection of geomorphological environmental changes using time-series Landsat images and grain size data: a case study in Baramarae tidal flats, Korea. Proceeding of Asian Conference on Remote Sensing, Bali, Indonesia, 133-137.

Lee, K.-S. and T.-H. Kim (2004). Topographic relief mapping on inter-tidal mudflat in Kyongki bay area using infrared bands of multi-temporal Landsat TM data. Korean Journal of Remote Sensing 20(3), 163-173.

Leon, J. X., G. B. M. Heuvelink and S. R. Phinn (2014). Incorporating DEM uncertainty in coastal inundation mapping. PLoS ONE 9(9), e108727, doi:10.1371/journal.pone.0108727.

Markham, B. L., J. C. Storey, D. L. Williams and J. R. Irons (2004). Landsat sensor performance: history and current status. IEEE Transactions on Geoscience and Remote Sensing 42(12), 2691-2694.

Mason, D. C., I. J. Davenport, R. A. Flather, B. McCartney and G. Robinson (1995). Construction of an intertidal digital elevation model by the 'water-line' method. Geophysical Research Letters 22(23), 3187-3190.

Mason, D. C., I. J. Davenport, R. A. Flather and C. Gurney (1998). A digital elevation model of the inter-tidal areas of the Wash, England, produced by the waterline method. International Journal of Remote Sensing 19(8), 1455-1460.

Noernberg, M. A., J. Fournier, S. Dubois and J. Populus (2010). Using airborne laser altimetry to estimate Sabellaria alveolata (Polychaeta: Sabellariidae) reefs volume in tidal flat environments. Estuarine, Coastal and Shelf Science 90(2), 93-102.

Park, J.-W., J.-H. Choi, Y.-K. Lee and J.-S Won (2012). Intertidal DEM generation using satellite radar interferometry. Korean Journal of Remote Sensing 28(1), 121-128. (in Korean, with English Abstract)

Park, N.-W. and D.-H. Jang (2014). Comparison of geostatistical kriging algorithms for intertidal surface sediment facies mapping with grain size data. The Scientific World Journal 2014, Article ID 145824, doi: 10.1155/2014/145824.

Park, N.-W., D.-H. Jang and K.-H. Chi (2009). Integration of IKONOS imagery for geostatistical mapping of sediment grain size at Baramarae beach, Korea. International Journal of Remote Sensing 30(21), 5703-5724.

Ryu, J.-H., J.-S. Won and K.-D. Min (2002). Waterline extraction from Landsat TM data in a tidal flat - A case study in Gomso Bay, Korea. Remote Sensing

of Environment 83(3), 442-456.

Ryu, J.-H., C. H. Kim, Y.-K. Lee, J.-S. Won, S.-S Chun and S. Lee (2008). Detecting the intertidal morphologic change using satellite data. Estuarine, Coastal and Shelf Science 78(4), 623-632.

Stockdon, H. F., A. H. Sallenger Jr., H. L. Jeffery and R. A. Holman (2002). Estimation of shoreline position and change using airborne topographic lidar data. Journal of Coastal Research 18(3), 502-513.

Van der Wal, D. and P. M. J. Herman (2007). Regression-based synergy of optical, shortwave infrared and microwave remote sensing for monitoring the grain-size of intertidal sediments. Remote Sensing of Environment 111(1), 89-106.

Van der Wal, D., P. M. Herman, R. M. Forster, T. Ysebaert, F. Rossi, E. Knaeps, Y. M. G. Plancke and S. J. Ides (2008). Distribution and dynamics of intertidal macrobenthos predicted from remote sensing: response to microphytobenthos and environment. Marine Ecology Progress Series 367, 57-72.

Wimmer, C., R. Siegmund, M. Schwäbisch and J. Moreira (2000). Generation of high precision DEMs of the Wadden Sea with airborne interferometric SAR. IEEE Transactions on Geoscience and Remote Sensing 38(5), 2234-2245.

Xu, Z., D.-J. Kim and S.-H. Kim (2013). Research of topography changes by artificial structures and scattering mechanism in Yoobu-Do inter-tidal flat using remote sensing data. Korean Journal of Remote Sensing 29(1), 57-68. (in Korean, with English Abstract)